Reactive Transport Modelling of NCG-Reinjection at Ngawha Geothermal Field

Vaibhav Rajput[1], Eylem Kaya[1], Bridget Lynne[1] and Dale E. Altar[1]

[1] Department of Engineering Science, University of Auckland, Private Bag 92019, Auckland, New Zealand

vraj882@aucklanduni.ac.nz

Keywords: *Reactive transport simulation, Ngāwhā geothermal field, NCG reinjection, TOUGHREACT™.*

ABSTRACT

Geothermal energy stands as a well-established, dependable, and sustainable source for generating electricity and providing district heating at lower temperatures. In striving to meet New Zealand's ambitious climate targets, geothermal power producers have taken bold steps to drastically reduce the country's carbon emissions. One noteworthy example is the Ngāwhā Geothermal plant operated by Top Energy, which initiated Non-Condensable Gases (NCGs) reinjection directly on site starting in May 2022 with OEC1. This innovative approach has since been expanded to other units as of early 2023, marking significant progress towards achieving carbon neutrality. This presents an interesting research question: exploring the effects of additional NCG reinjection on key reservoir parameters through a comprehensive modelling study for Ngāwhā field.

Reservoir modelling is crucial in comprehending how fluids move within geothermal reservoirs. However, very few studies are performed that incorporate the chemical interaction occurring between fluid and rock insitu. To understand what happens to injected NCGs and how it chemically alters the reservoir, conducting reactive transport modelling becomes essential. This approach provides detailed insights into how these changes evolve spatially and over time. Such information is crucial for effectively managing resources and gaining confidence in our understanding of the complex thermal, hydraulic, and chemical processes occurring underground.

In this study, 1D numerical models were set up to address the above research aims. One of the primary reinjection wells, NG11, was chosen for detailed analysis. A 1D MINC radial model was generated in TOUGHREACT4™ using publicly accessible information on Ngāwhā field. The MINC approach was selected to represent the highly fractured nature of the Ngāwhā field more accurately. The results from our study provide insights into the principal minerals expected to dissolve and/or precipitate, the subsequent changes on porosity and permeability, and effect of injected CO_2 for various scenarios. Three different reinjection scenarios were modelled, and the results suggest that calcite dissolution increases with higher NCG reinjection content. Out of the others minerals considered, pyrite, illite, and albite showed strong tendency for precipitation. Due to the high dissolution rate of calcite compared to other minerals, its effect on overall change in porosity was profound, which led to an increase in porosity. Significantly, the injected CO_2 stayed in the aqueous phase due to non-precipitation of calcite and other carbonate minerals.

1. INTRODUCTION

Geothermal energy is a mature, baseload, and renewable energy source for electricity generation and low-temperature district heating usage. Due to New Zealand's unique location and access to some of the best geothermal sites worldwide, it contributed about 8,033 GWh or 18.47% of the total electricity generation in the country for calendar year 2022 (MBIE, 2023). However, the industry has come under lenses recently due to the government's emphasis on reducing carbon emissions, in particular from the electricity generation sector. Although the average median emissions from geothermal sources in New Zealand is ~64 gCO_{2e}/kWh and is considerably lower than fossil fuel generators, it can still be higher than those of other renewable energy sources, depending on specific lifecycle factors. However, the emissions vary widely within different geothermal sites in New Zealand, with the lowest emitters being Wairakei (29 gCO_{2e}/kWh) and Mokai (35 gCO_{2e}/kWh) and the largest being Ohaaki (292 gCO_{2e}/kWh) and Ngāwhā (172 gCO_{2e}/kWh) (McLean, 2023).

Non-condensable gases (NCGs) flow with reservoir fluids to surface and are routinely separated to generate high-quality steam to be fed into power station turbines. NCG separation is commonly performed using liquid ring vacuum pumps, steam ejectors, and centrifugal compressors. This separation process is necessary to improve the turbine efficiency. Until recently, most geothermal plant operators used to vent these separated NCGs (mainly CO_2) into the atmosphere. However, with the government focus on reducing emissions from energy sector and the substantial carbon abatement fees amounting millions of dollars annually (Northland Regional Council, 2023), it has become imperative for the geothermal operators to address these concerns. Consequently, the geothermal industry is actively exploring strategies for reinjecting produced NCGs back into the reservoir or finding ways to utilise them industrially. Ngāwhā generation site, which is operated by Top Energy, has emerged as the leader in this initiative and reinjected 100% of the NCGs in the year 2023 (McLean, 2023; Northland Regional Council, 2023). While it is not fully clear what specific engineering studies Top Energy may be conducting on the physical/chemical effects of NCG reinjection, there remains a gap in publicly available research on the reservoir and surface behaviour. This research aims to carry out this analysis, which will help to improve our understanding of effects of NCG reinjection on geothermal fields in general and Ngāwhā field in particular.

1.2 Research Goals

Through this study, it is desired to address the following questions:

- What changes might occur to rock properties (e.g. porosity and permeability) due to hydrothermal alteration? Which minerals can potentially dissolve or precipitate?
- What will happen to the reinjected CO_2 and H_2S? Will it mineralize or stay in dissolved state?

There have been recent studies (Titus et. al., 2024) conducted on injecting biogenic CO_2 at Ngāwhā geothermal field (NGF) from a theoretical standpoint. Others have completed modelling studies for fields in Iceland (Ratouis et. al., 2022), where similar to Ngāwhā field, the NCG reinjection is taking place. However, these studies do not take into account the geochemical interaction occurring between injected fluid and surrounding rock structure through which it travels (Siahaan et al., 2024; Ruiz et al., 2021; Xu et al., 2003; Xu et al., 2004). Utilizing a reactive transport simulator, several model scenarios were implemented to predict the potential effects of NCG reinjection on mineral precipitation and dissolution, and to estimate the subsequent changes on porosity and permeability.

2. REACTIVE TRANSPORT MODEL

For this study, the numerical simulation tool TOUGHREACT4™ is used for setting up the model. TOUGHREACT4™ is a fluid flow and geochemical transport simulation tool developed by combining reactive chemistry with the flow simulation framework of TOUGH2™ (Pruess et al., 1999; Sonnenthal et al., 2021). The fluid equation of state EOS1 was selected since it can handle dissolved CO_2, which aligns with the current conditions in the geothermal reservoir. However, EOS1 is limited to dissolved gases and does not account for multiphase mixtures of water and CO_2. If the long-term scenarios indicate that the amount of dissolved gases increases to a level where this assumption is no longer valid, the model will need to be converted to a more appropriate EOS module that can accurately simulate the behavior of free CO2 in the reservoir. PyTOUGH was utilised to create model grids and input files, and to visualize output results (Croucher, 2011; Croucher, 2015).

2.1 Flow Parameters

As this study is based on publicly available information about NGF, we decided to choose a reinjection well with sufficient information on mineral assemblage and flow rate to investigate the ongoing mineral alteration process at NGF. Both reinjection wells NG11 and NG18 fit these criteria, and thus NG11 was chosen for further evaluation. A 1D radial model was created using PyTOUGH code. The model has 100 gridblocks. The first gridblock, representing the injection point, was set at 0.1m. Gridblock sizes were then increased logarithmically, with the largest cell size is 2000 m. The model boundaries were extended up to 20.01 km to ensure model is large enough to prevent artifacts caused by boundary conditions. E.g. this extension ensures that the effects of injection will be not be felt at the outer limits of the boundary, thereby avoiding any distortions in the results. Additionally, the top boundary was considered as closed, whereas an upflow flux rate of 2.0E-5 (kg/s)/m^2 was considered at bottom boundary.

NG11 has two feed zones, located at approximately 900 m and 1050 m (Cox and Browne, 1998). The bottom feed zone is the dominant one, with the thickness of 80 m (1010 m to 1090 m). This feed zone contribution is taken to be 75% of the total fluid intake.

A dual porosity multiple interaction continua (MINC) model was selected for grid structure. NGF, in contrast to fields in TVZ, is highly fractured, with fracture density of 15 per meter (Browne, 1980). The fluid flow travels mainly through these fractures while matrix elements act as storage. In this study, a single continuum was used for the matrix, and one for fractures, constituting a dual porosity model (Pruess et. al., 1999). This approach is chosen because the MINC model more accurately represents the fractured nature of the greywacke and argillite in the NGF reservoir. The MINC grid structure was implemented within the first 5.4 km from the injection well (approximating the MT boundary of NGF), while the rest of the model was assumed to be a single porosity continuum. Additional MINC parameter values are shown in Table 1.

Table 1: MINC parameter values (Browne, 1981; Kaya, 2002)

Parameter	Value
Fracture density	15 per meter
Fracture porosity	0.9
Matrix porosity	0.08
Fracture permeability (horizontal and vertical)	100.00E^{-15} m^2
Matrix horizontal permeability	5.00E^{-15} m^2
Matrix vertical permeability	1.00E^{-15} m^2
Volume fraction of the fracture continuum	2%

In the first phase, the model is run for 23 years, to represent the period from the start of injection in 1998 through 2021, with no active NCG reinjection during this time. In the second phase, three scenarios are considered over the subsequent 20 years:

- No active reinjection of NCG (Case A)
- Active reinjection of 50% of total NCG emission released (Case B)
- Active reinjection of 100% of total NCG emission released (Case C)

2.2 Geochemical Parameters

2.2.1 Initial and Boundary Water Chemistry

The initial water and boundary water chemistry are shown in Table 2. The initial water chemistry profile was obtained from Sheppard (1987). The boundary water for case A was assumed to be similar to the initial water, with the only difference being the vented NCGs. In the real case scenario, the CO_2 concentration would be determined by the temperature and pressure values at the actual separation point between NCG and brine. Due to unavailability of this information, for case A, it was assumed that the NCG passive reinjection was 18% of the total produced NCG (Ruiz et al, 2021), while a single cell TOUGHREACT model was used to estimate the fluid's chemical components at surface conditions using the discharge gas fraction from Sheppard (1987). For cases B and C, the boundary water is the same as for case A for the first 23 years, while it is replaced by another chemistry with an assumption of 0.3% wt. and 0.6% wt. of CO_2. This would reflect the CO_2 mass fraction observed in production wells at NGF, as reported by Burnell et al. (2016). The reported values of the ratio of CO_2/H_2S by Bromley and Bignall (2016) were used to calculate and incorporate the concentration of H_2S in the model. Based on the weight percentage of CO_2 for different reinjection cases, the concentration of H_2S is estimated. However, since the ratio is decreasing with time along with the CO_2 concentration, the H_2S content remains approximately constant.

ISSN 2703-4275

Table 2: Initial and Boundary Water Chemistry Input (adapted from Sheppard, 1987)

Primary Species	Water Concentration Profile (mol/kg)			
	Initial Water	Boundary Water – Passive Reinjection (Case A)	Boundary Water – 50% Reinjection (Case B)	Boundary Water – 100% Reinjection (Case C)
h+	9.793E-07	1.585E-07	3.162E-07	6.310E-07
na+	4.112E-02	3.810E-02	3.810E-02	3.810E-02
k+	1.989E-03	1.996E-03	1.996E-03	1.996E-03
ca+2	1.233E-04	6.238E-05	6.238E-05	6.238E-05
sio2(aq)	1.571E-02	6.557E-03	6.557E-03	6.557E-03
so4-2	2.590E-04	2.599E-04	2.599E-04	2.599E-04
hco3-	2.804E-01	2.454E-02	6.817E-02	1.363E-01
h2s(aq)	3.750E-03	3.168E-04	3.929E-03	3.929E-03
h2(aq)	6.694E-04	4.776E-05	1.433E-04	2.865E-04
o2(aq)	5.118E-07	4.729E-09	1.419E-07	2.837E-07
alo2-	3.298E-04	3.305E-05	3.305E-05	3.305E-05
fe+2	2.055E-06	1.528E-06	1.528E-06	1.528E-06
mg+2	1.655E-05	5.348E-06	5.348E-06	5.348E-06

Bottom heat and mass flux was accounted for through the fracture blocks. The boundary water chemistry to represent this natural flux was set to be equal to the initial water chemistry and the fluid enthalpy was set to 955 kJ/kg, corresponding to temperature of 223°C. The upflow rate is set to 10 kg/s, which is based on the estimates of the total mass flow from surface heat flow measurements, and adjustments made during numerical experiments and model calibration (Burnell, 2016).

2.2.2 Initial Mineral Assemblage and Mineral Reaction Parameters

The Permian-Jurassic Waipapa Group, comprising mainly of a succession of quartzo-feldspathic greywackes and argillites, forms the host rock of NGF as well as its basement (Cox and Browne, 1998; Melia et al., 2022). The mineral assemblage and the individual volume fractions for NG11 are based on the work by Cox (1985) and Browne and Gartner (1982), and summarized in Table 3. Core and cutting samples were analyzed from different wells and at different depths for each well. The minerals are categorised into primary minerals (minerals which are known to exist) and secondary minerals (or minerals which can potentially form due to hydrothermal alteration). The volume fractions for secondary minerals are assigned a value of 0.0.

Table 3: Mineral volume fractions for NG11 (Cox and Browne, 1998)

	Minerals	% Vol
Primary	Calcite	10.5%
	Quartz	34.7%
	Pyrite	4.4%
	K-feldspar	4.7%
	Albite	6.4%
	Muscovite	4.8%
	Chlorite	11.2%
	Illite	4.8%
	Biotite (Annite)	1.2%
Secondary	Smectite, Siderite, Prehnite, Am Silica, Epidote, Montmorillonite, Magnesite, Wairakite	

The mineral kinetic rate parameters were adapted from Palandri & Kharaka (2004). Biotite was approximated by its end-member, annite in the chemical input file. All mineral dissolution/precipitation process were modelled under kinetic conditions. Although calcite dissolution is known to proceed at a fast rate at lab conditions, it was not considered at equilibrium, due to the field rates being a few orders of magnitude smaller than the lab-derived rates. The kinetic rate constants used are presented in Table 4.

Table 4: Kinetic rate constant information for different minerals (Palandri & Kharaka, 2004)

Mineral	Acid dissolution			Neutral		Other dissolution		
	log k25	Ea	Reaction order	log k25	Ea	log k25	Ea	Reaction order
Calcite	-0.3	14.4	1	-5.81	23.5	-3.48	35.4	1[a]
Quartz				-13.99	87.7	-16.29	108360	-0.5
Feldspar	-10.06	51.7	0.5	-12.41	38	-21.2	93.9	-0.822
Albite	-10.16	65	0.457	-12.56	69.8	-15.6	71	-0.572
Chlorite	-11.11	88	0.5	-12.52	88			
Epidote	-10.6	71.1	0.337	-11.99	70.7	-17.33	79.1	-0.556
Muscovite	-11.85	22	0.368	-13.55	22	-14.55	22	-0.22
Biotite	-9.84	22	0.525	-12.55	22			
Smectite	-10.98	23.6	0.34	-12.77	35	-16.52	58.9	-0.4
Prehnite	-10.66	80.5	0.256	-13.16	93.3	-14.86	93.3	-0.2
Siderite[b]				-8.90	62.7			
Pyrite[d]	-7.52	56.9	-0.5	-4.55	56.9			
Illite[c]				-12.6	14			
Montmorillonite	-12.71	48	0.22	-14.41	48	-14.41	48	-0.13
Magnesite	-6.38	14.4	1	-9.34	23.5	-5.22	62.8	1
Wairakite[e]				-13.0	54.4			
Am. Silica				-12.77	68.7			

[a] Reaction order with respect to CO_2
[b] Rate constants adapted from Xu et. al. (2005)
[c] Rate constants adapted from Köhler et al. (2003)
[d] Neutral mechanism with respect to O_2 and reaction order of 0.5
[e] Rate constants adapted from Todaka et. al. (2004)

The kinetic dissolution or precipitation of minerals in TOUGHREACT4™ is represented by the general Transition State Theory (TST) rate law based on the work of Lasaga (1998). In this equation, k_n is the rate constant (moles per unit surface area and unit time), A_n is the reactive surface area (m^2/kg), Ω_n is the mineral saturation ratio, while θ and η are experimental rate constants (which are usually taken as equal to one) (Sonnenthal et al., 2021).

$$r_n = \pm k_n A_n \left|1 - \Omega_n^{\theta}\right|^{\eta} \quad (1)$$

where positive values of r_n indicate dissolution and negative values indicates precipitation.

In TOUGHREACT4™, apart from the rate constants (k), the other variable that can be used to adjust the reaction kinetics is the mineral reactive surface area (RSA). The latter approach is preferred by some authors (Altar et al., 2022), since it allows variation of the parameter that already has a large range of uncertainty. This approach also allows using the rate constants from published literature, since these are usually measured quantities.

The estimation of fracture and matrix RSA parameters is explained in detail in the appendix of TOUGHREACT user manual (Sonnenthal et al., 2021). For the mineral assemblage considered, the RSA values for fracture continuum ranged from 4.24E-05 to 1.47E+01 $m^2_{\text{reactive surface}}/m^3_{\text{total fracture medium}}$. For matrix however, a simplifying assumption was used and the RSA values for all minerals were uniformly set to 1.0E+03 $m^2_{\text{mineral}}/m^3_{\text{mineral}}$.

To estimate the effect of mineral abundance variation on permeability, it is essential to model the permeability as a function of initial permeability and porosity changes. This relationship in fracture continua is approximated by Verma-Pruess relation (Verma and Pruess, 1988). The critical porosity was set to 0.05 and the exponent was set to a value of 2. Carman-Kozeny relation was used for matrix continua.

3. RESULTS

Due to their high kinetic dissolution/precipitation rates, it is found that calcite (and to an extent, pyrite, illite, albite) have high influence over the changes in porosity due to mineral abundance changes. A comparison is made between case A (no active reinjection), case B (50% reinjection), and case C (100% reinjection) at the end of 20 years of operation or year 2041. This is shown in Figure 1 to Figure 4. Visually, it can be observed that calcite dissolution, pyrite precipitation, and overall increase in fracture porosity are enhanced going from passive reinjection to 100% NCG reinjection cases. At the end of passive reinjection in 2041, calcite dissolution and pyrite precipitation has taken place. Corresponding changes in porosity can also be observed. An overview of pH variation in Figure 3 shows that it is quite uniform for the MINC model. This can be attributed to the fact that, in case of MINC, fluid movement takes place through highly permeable fractures which helps in the uniformity of pH.

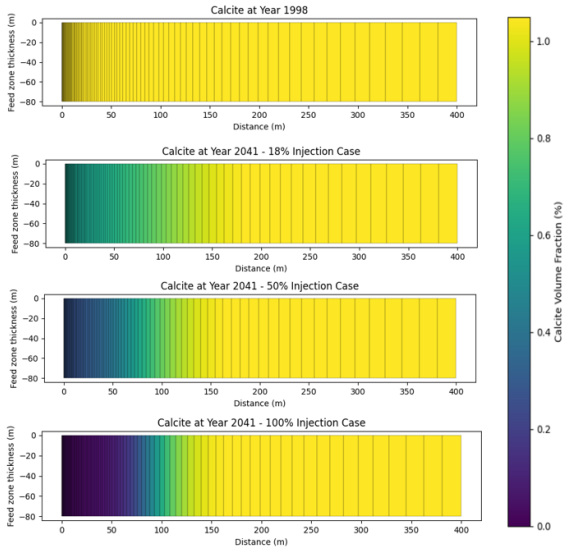


Figure 1: Variation in calcite over model extent at year 1998 and 2041 for Case A, B, and C

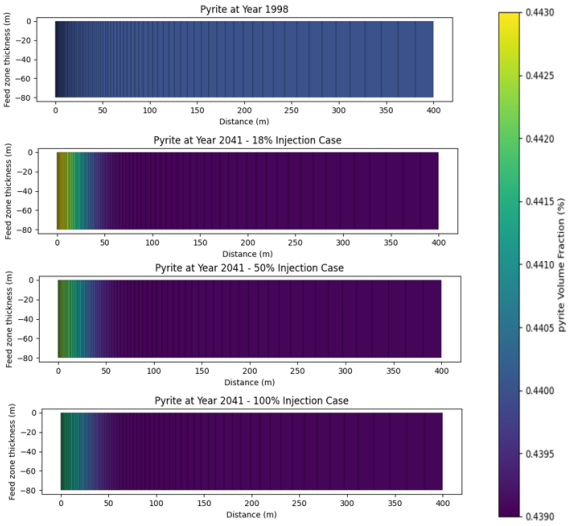


Figure 2: Variation in pyrite over model extent at year 1998 and 2041 for Case A, B, and C

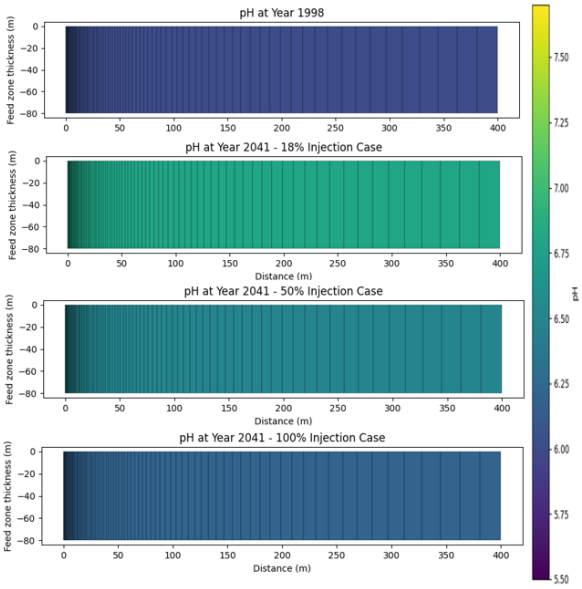


Figure 3: Variation in pH over model extent at year 1998 and 2041 for Case A, B, and C

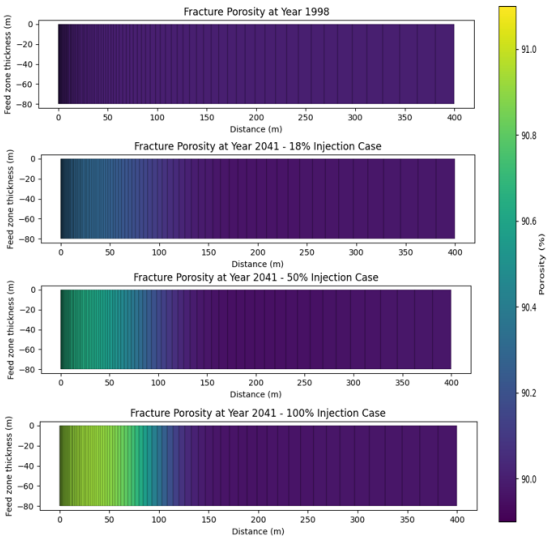


Figure 4: Variation in porosity over model extent at year 1998 and 2041 for Case A, B, and C

It is observed that a majority of the mineral abundance (and thus, porosity) changes occur within a few hundred meters from the reinjection well. Thus, the same results could be plotted on a semi-log scale to better visualize the changes, shown in Figure 5 and Figure 6.

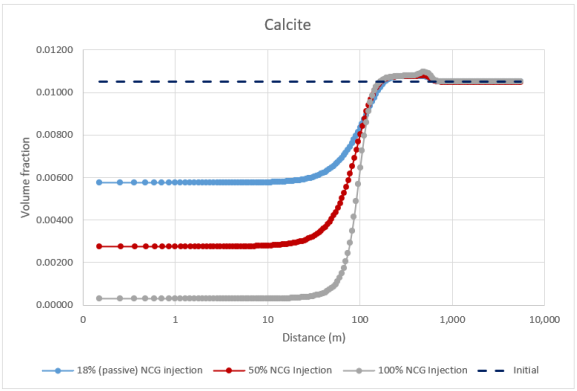


Figure 5: Variation in calcite abundance over model extent (at year 2041) for Case A, B, and C

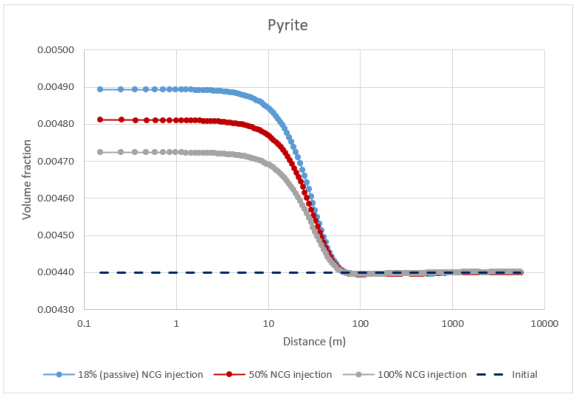


Figure 6: Variation in pyrite abundance over model extent (at year 2041) for Case A, B, and C

It is observed that, passive reinjection of NCG causes dissolution of calcite in fractures. The intensity of dissolution increases with an increase in NCG content (and subsequent increase in pH), with the highest dissolution found for 100% reinjection (case C). For a distance of up to 16 m from the injection well, 45% of calcite dissolves for case A. while 73.6% and 97.2% dissolve in Cases B and C, respectively. The total extent of dissolution or chemical front reaches about 167 m from the well. From 167 m to 677 m, calcite precipitation takes place. If a production or monitoring well is placed within this distance, it could confirm and quantify this calcite precipitation. Thermodynamic conditions, along with chemical and pH changes over the evolution of the alteration process, favor precipitation at this distance.

Following calcite dissolution, the dissociated bicarbonate ions either stay in aqueous phase or are taken up in forming magnesite and siderite. There is no precipitation of siderite and the precipitation of magnesite is very minimal as compared to the amount of calcite being dissolved as a whole. Thus, a majority of dissolved bicarbonate as well as reinjected CO_2 stays in aqueous phase. This is also visible in the bicarbonate concentration in aqueous phase shown in Figure 7.

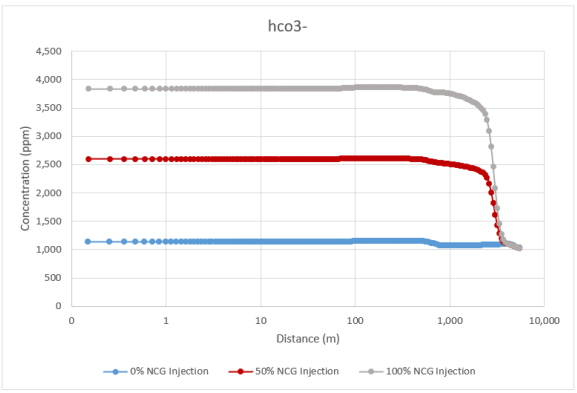


Figure 7: Variation in bicarbonate concentration in aqueous phase over model extent (at year 2041) for Case A, B, and C

Pyrite undergoes precipitation, with the rate of precipitation is highest for passive reinjection (case A), and decreases with additional NCG content. The formation of pyrite is controlled by Fe^{+2} and $H_2S_{(aq)}$ concentrations. The other minerals that depend upon these ions, and those that could potentially affect pyrite precipitation rates are biotite (represented by end member annite in our case), chlorite, siderite, and epidote. Siderite, which is a secondary mineral, does not precipitate during the entire run. Chlorite, a primary mineral, undergoes precipitation itself for roughly 1000 m from the well location for all the cases (presented in Figure 8). Annite (secondary mineral) also undergoes precipitation, but it starts forming about 400 m away from the well, thus possibly not interfering in pyrite formation. Epidote (a primary mineral) does precipitate along the entire length of the reservoir, but the amount of precipitation is very small. Thus, among the minerals considered affecting pyrite formation rates, only chlorite seems to be the mineral that competes with pyrite for Fe^{+2} ions.

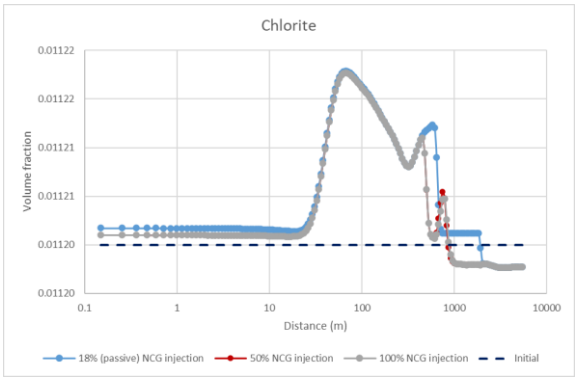


Figure 8: Variation in chlorite abundance over model extent (at year 2041) for Case A, B, and C

Among the other minerals, the largest changes in abundances are observed for illite and albite, presented in Figure 9 and Figure 10, respectively. Illite, whose formation depends upon magnesium, potassium and aluminium ions, undergoes highest precipitation for passive reinjection, while the formation rate decreases with increasing NCG content. This mineral continues to form a bit farther than the chemical front at about 300 m. Albite is a special case, because it undergoes precipitation from the well location till about 200 m, and thereafter undergoes dissolution. It is the only mineral among those considered that depend upon sodium ions for its

formation. Similar to illite, this mineral shows highest precipitation for case A, and diminishing rates for higher NCG content.

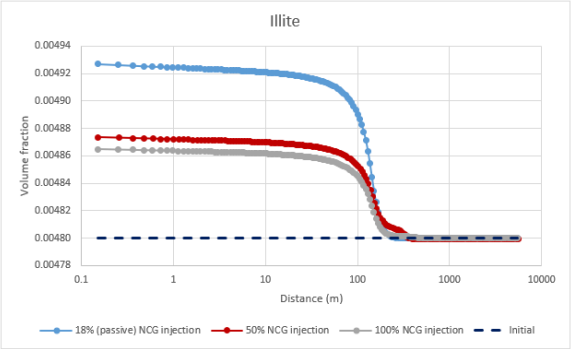


Figure 9: Variation in illite abundance over model extent (at year 2041) for Case A, B, and C

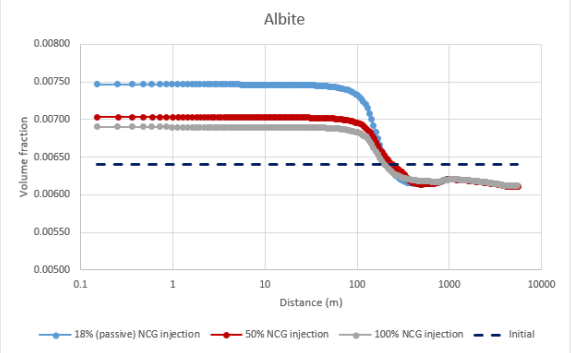


Figure 10: Variation in albite abundance over model extent (at year 2041) for Case A, B, and C

Thus, the calcite dissolution has a large effect on the net change in mineral volume fractions, and this leads to increase in porosity for all three cases considered (Figure 11). This correspondingly increases the permeability in fractures, shown in the same figure.

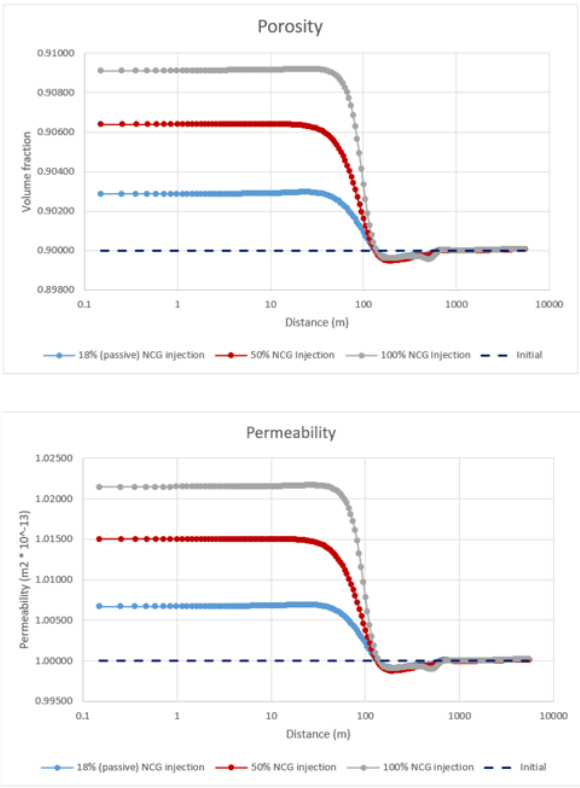


Figure 11: Variation in fracture porosity and fracture horizontal permeability over model extent (at year 2041) for Case A, B, and C

4. CONCLUSIONS

We have developed a 1D radial MINC model for the feed-zone of a NGF reinjection well (NG11) using the reactive transport modeling tool, TOUGHREACT4™. This model incorporates thermodynamic conditions and fluid-rock interactions. By utilizing the data sourced from the literature, the mineral assemblage was carefully selected to reflect the actual minerals present at the main feed zone of NG11 and this was combined with the publicly available fluid chemistry data. The model was used to assess changes in mineral abundances due to NCG reinjection, and its subsequent effect on rock properties.

For the different reinjection cases considered, the results suggest that calcite dissolution takes place mainly for fracture continua for all three cases, with the rate of dissolution increasing as the NCG content increases.

Pyrite, chlorite, illite, and albite were the other key minerals that precipitated. Among the secondary minerals, smectite had the largest rate of precipitation. However, calcite still had the highest contribution to the net change of mineral abundances, which caused an increase in fracture porosity and permeability of the system. Injected CO_2 stays mostly in aqueous phase in bicarbonate form, and does not mineralize into calcite, magnesite or siderite in the area nearby the injection well. Small scale precipitation of these minerals is observed from 167 m to 677 m distance. H_2S, however, mineralized in the form of pyrite till about 80 m from injection well.

Further continuation of this study would be to evaluate the results in more detail with the help of a larger scale model and incorporating real field data that reflects the recent conditions

of the field. This can include incorporating tracer tests into the model to enhance the accuracy. Although the 1D approach provided insights into the overall effects on mineral abundances due to NCG reinjection, a large-scale model would consider additional complexities, such as flow effects related to hydraulic connections between injection and productions wells in the field, different rock types and their lithologies with different mineral assemblages, potential breakthrough of injected NCG to the production wells, among others. Implementing the EOS2 or ECO2N module of TOUGHREACT would improve the investigation of long-term structural trapping potential and allow for a more comprehensive assessment of surface leakage risks.

Understanding how NCG injection affects caprock strength and permeability is also important to evaluate the long-term sustainability and impacts on surface features.

ACKNOWLEDGEMENT

The first author wishes to acknowledge and thank the University of Auckland for providing the "University of Auckland India High Achievers Scholarship" during the author's course completion. We also thank the NZ Ministry of Business, Innovation and Employment for funding the work through MBIE Research Programmes: UOAX2211 "Reversing Carbon Emissions in the Geothermal Energy Industry: Template for Emission-Intensive Industries" projects and C05X1904 "Geothermal: the Next Generation".

REFERENCES

Altar, D. E., Kaya, E., Zarrouk, S. J., Passarella, M., and Mountain, B. W. (2022). Numerical geochemical modelling of basalt-water interaction under subcritical conditions. Geothermics, 105, 102520-. https://doi.org/10.1016/j.geothermics.2022.102520.

Bromley, C., and Bignall, G. (2016). Ngawha Geothermal Field: Geology, Geophysics, Conceptual Model, Geochemical Monitoring Trends & Environmental Issues. JOGMEC-GNS Workshop, Tokyo, 2nd June, 2016.

Browne, P. R. L. (1980) Joint channels in reservoir rocks of the Ngawha geothermal field, Northland, New Zealand. N. Z. Geothermal Workshop, Proc. Univ. Auckland, pp. 81-84.

Browne, P. R. L. and Gardner, M. W. (1982) Subsurface alteration at the Ngawha geothermal field: a progress report. Pacific Geotherm. Confer. and N. Z. Geotherm. Workshop, Proc., Univ. Auckland, pp. 39-44.

Burnell, J., Weir, G., and Kissling, W. (2016). MODELLING THE NGAWHA GEOTHERMAL FIELD. Proceedings of the 38th New Zealand Geothermal Workshop.

Burnell, J. (2016). Statement of Evidence of Dr. John Burnell for Northland Regional council and Far North District Council Hearing Concerning a Resource Consent Application by Ngawha Generation Ltd for Expanded of Ngawha Geothermal Field; Public Hearing in Kerikeri on 10-14 August 2015. GNS Science Report 2016/08.

Cox, M. E., and Browne, P. (1998) "Hydrothermal Alteration Mineralogy as an Indicator of Hydrology at the Ngawha Geothermal Field, New Zealand." Geothermics 27.3: 259–270.

Cox, M. E. (1985) Geochemical examination of the active hydrothermal system at Ngawha, Northland, New Zealand: hydrochemical model, element distribution and geological setting. PhD dissertation, Univ. Auckland, 385 pp.

Croucher, A.E., 2011. PyTOUGH: a Python scripting library for automating TOUGH2 simulations. In: Proceedings, New Zealand Geothermal Workshop 2011. Auckland, New Zealand.

Croucher, A., 2015. Recent developments in the PyTOUGH scripting library for TOUGH2 simulations. In: Proceedings, 37th New Zealand Geothermal Workshop. Taupo, New Zealand.

Kaya, E. (2002). Modeling of Production Behaviour of Ngawha Geothermal Field, New Zealand. Report submitted to The University of Auckland.

Köhler, S. J., Dufaud, F., & Oelkers, E. H. (2003). An experimental study of illite dissolution kinetics as a function of ph from 1.4 to 12.4 and temperature from 5 to 50°C. Geochimica et Cosmochimica Acta, 67(19), 3583–3594. https://doi.org/10.1016/S0016-7037(03)00163-7

Lasaga, A.C., 1998. Kinetic Theory in the Earth Sciences. Princeton University Press, Princeton, New Jersey

McLean, K. (2023). Updates from NZGA Emissions Working Group. New Zealand Geothermal Association Presentation at NZGW Winter Seminar 2023, Taupo, NZ

Melia, A., Faulkner, D. R., & McNamara, D. D. (2022). Physical property characterization of the Waipapa greywacke: an important geothermal reservoir basement rock in New Zealand. Geothermal Energy, 10(1), 1–25. https://doi.org/10.1186/s40517-022-00218-2

Northland Regional Council. (28 August, 2023). Ngāwhā Generation Ltd – Zero Carbon Electricity for the Far North. https://www.nrc.govt.nz/our-northland/story/?id=77730

Palandri, J.L., Kharaka, Y.K. (2004). A Compilation of Rate Parameters of Water-Mineral Interaction Kinetics for Application to Geochemical Modeling. U.S. Geological Survey, Menlo Park, California

Pruess, K., Oldenburg, C.M., Moridis, G.J. (1999). TOUGH2 User's Guide Version 2. Lawrence Berkeley National Laboratory.

Ratouis, T. M. P., Snæbjörnsdóttir, S. Ó., Voigt, M. J., Sigfússon, B., Gunnarsson, G., Aradóttir, E. S., & Hjörleifsdóttir, V. (2022). Carbfix 2: A transport model of long-term CO2 and H2S injection into basaltic rocks at Hellisheidi, SW-Iceland. International Journal of Greenhouse Gas Control, 114, 103586. https://doi.org/10.1016/j.ijggc.2022.103586

Ruiz, N. C., McLean, K., Richardson, I., Misa, T., Ferguson, A., Altar, D. E., and Kaya, E. (2021). Passive NCG

Reinjection at Te Huka Geothermal Binary Power Plant. Proceedings of the 43rd New Zealand Geothermal Workshop, 2021.

Sheppard, D.S. (1987). Geochemistry and the Exploration of the Ngawha Geothermal System, New Zealand. Proceedings of the 22nd New Zealand Geothermal Workshop, 2000

Siahaan, Y., Kaya, E., Altar, D., Mering, J., Subekti, D., Utami, A., Atayde, R., Melia K., Sepulveda, F., (2024) Reactive Transport Modelling of Fluid-NCG Reinjection in Ngā Tamariki Geothermal Field, New Zealand, Proceedings 46th New Zealand Geothermal Workshop, 20-22 November, 2024, Auckland, New Zealand, ISSN 2703-4275

Sonnenthal, E., Spycher, N., Xu, T., and Zheng, L. (2021) TOUGHREACT V4.12-OMP and TReactMech V1.0 Geochemical and Reactive-Transport User Guide. Lawrence Berkeley National Laboratory.

Titus, K., Dempsey, D., Peer, R., & Hanik, F. (2024). From carbon neutral to carbon negative: a theoretical bioenergy and CO2 removal retrofit at Ngāwhā geothermal power station. Journal of the Royal Society of New Zealand, 1–19. https://doi.org/10.1080/03036758.2024.2385807

Todaka, N., Aasaka, C., Xu, T., and Pruess, K. (2004) Reactive geothermal transport simulations to study the formation mechanism of an impermeable barrier between acidic and neutral fluid zones in the Onikobe Geothermal Field, Japan. Journal of Geophysical Research, 109.

Verma, A., and Pruess, K. (1988) Thermohydrological conditions and silica redistribution near high-level nuclear wastes emplaced in saturated geological formations, J. Geophys. Res., v. 93, p. 1159-1173.

Xu, T., Apps, J. A., & Pruess, K. (2003). Reactive geochemical transport simulation to study mineral trapping for CO2 disposal in deep arenaceous formations. *Journal of Geophysical Research - Solid Earth*, *108*(B2), 2071-n/a. https://doi.org/10.1029/2002JB001979

Xu, T, Apps, J. A., and Pruess, K. (2004). Numerical simulation of CO2 disposal by mineral trapping in deep aquifers, Applied Geochemistry, v. 19, p. 917-936, 2004.

Xu, T., Apps, J. A., & Pruess, K. (2005). Mineral sequestration of carbon dioxide in a sandstone–shale system. Chemical Geology, 217(3), 295–318. https://doi.org/10.1016/j.chemgeo.2004.12.015

.